LIGO SURF

Final Paper # 09212023

Estimation of the Stochastic Gravitational Wave Background from binary mergers

By Pritvik Sinhadc
Undergraduate student pursuing Bachelor of Science in Physics
The Division of Physics, Mathematics and Astronomy
California Institute of Technology
psinhadc@caltech.edu
pritvik.sinhadc@LIGO.org

Mentors:

Dr. Alan Weinstein
Professor of Physics
The Division of Physics, Mathematics and Astronomy
California Institute of Technology
ajw@caltech.edu

Dr. Patrick Meyers
Postdoctoral Scholar Research Associate in Physics
The Division of Physics, Mathematics and Astronomy
California Institute of Technology
pmeyers@caltech.edu

Dr. Arianna Renzini
Postdoctoral Scholar Research Associate in Physics
The Division of Physics, Mathematics and Astronomy
California Institute of Technology
arenzini@caltech.edu

Abstract
The ground-based International Gravitational-Wave Observatory Network (IGWN), including the Laser Interferometer Gravitational-Wave Observatory (LIGO) stations at Hanford and Livingston, Virgo and KAGRA [1], has detected gravitational waves (GWs) from Compact Binary Coalescence (CBC) sources [2] in distant galaxies as far away as 8 Gigaparsecs [3], which corresponds to a redshift of slightly greater than 1. More distant sources are too faint to be confidently detected as individual events. However, they are expected to be so numerous that they can be detectable as a Stochastic Gravitational Wave Background (SGWB) [4]. While stringent upper limits on the strength of the SGWB as a function of frequency in units of the cosmological closure density of the universe, $\Omega_{GW}(f)$ [5], have been made through the IGWN, there has been no observed detection of the SGWB as such. However, while this was overturned as per the June 28, 2023, announcement on the preliminary — not completely confirmed — detection of an SGWB, which is believed to come from supermassive black hole mergers, the astrophysical background from all CBC sources in the LIGO frequency band is still to be detected [15]. Early implications for the SGWB from the first observation of stellar-mass Binary Black Hole (BBH) mergers [6] and more recent models from advanced LIGO and VIRGO data [7, 8] have all provided estimates of the CBC merger rate, which suggest that we are close to detecting the SGWB. The estimates from the 'Regimbau method' [6] come from complex simulations of many individual events, while the 'Callister method' [7] is based on numerical evaluation on an analytical expression for the SGWB. We reproduce these estimates through a thorough analysis of the methods used by Regimbau and Callister [6, 7], and study the degree to which they agree with each other, as well as the extent to which the results depend on uncertainties in the merger rate as a function of mass and redshift distributions of the sources. Overall, we investigate the predictions on SGWB parameters and constrain its limits, thereby decoding how the background changes due to uncertainties in several important astrophysical parameters. This incorporation of the latest theoretical models, with a key understanding of the limits and constraints in these frameworks, will aid in the long-term goal of refining estimates on the SGWB and detecting them with the IGWN.

GW science: An introduction
The principles of general relativity, specifically the link between the spacetime metric as described by Einstein field equations and energy-momentum tensor, including matter, momentum and stress, show that acceleration of massive objects creates warping or distortions in the fabric of spacetime. This phenomenon of spacetime curvature can propagate through space as a GW in a manner analogous to electromagnetic or even fluid waves spreading out from a source [2].

All GWs that have been detected by the IGWN to date are attributed to CBCs [3], specifically the merger of compact, stellar mass objects [1], which include events such as the merger of two neutron stars or two black holes [3] or a black hole and a neutron star [1, 3]. During such events, a portion of the mass energy and kinetic energy of the merging objects is converted into GWs, which emanate from the merging site and progressively reduce in amplitude. Analogous to conventional waves, these GWs carry information on the original source via frequency, wavelength, and amplitude [1]. According to general relativity, it is worth noting that GWs warp

space-time as they propagate due to the fundamental interplay between spacetime curvature, matter-energy distribution, and momentum.

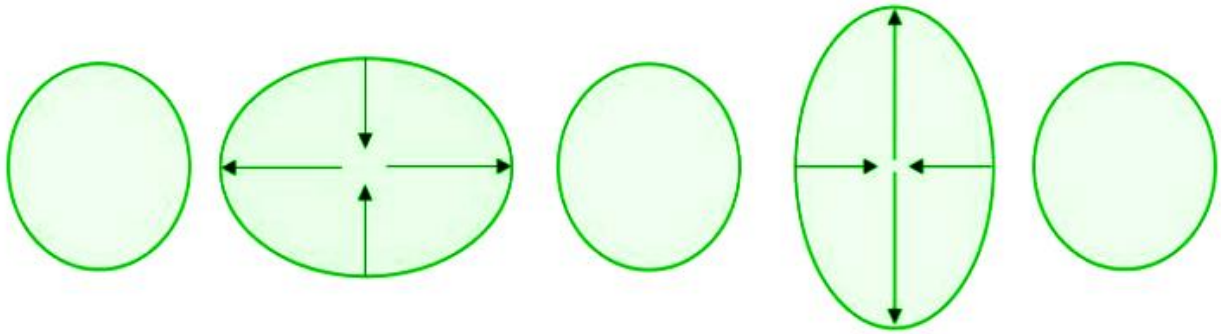

Figure 1: This figure illustrates the deformation of the space-time fabric within an object induced by the passage of a GW, with each image representing a distinct stage in the warping. The object oscillates from maximum longitudinal stretching to maximum latitudinal stretching, with arrows showing the direction of warping of the spacetime fabric. Such a warping is described as linearly polarized. In this case, the effect is exaggerated, since by the time such waves are detected by the IGWN, the warping caused by them results in extremely small changes in distance — less than 1/1000th the diameter of a proton [2].

Source: Image generated by the author.

This present overview holds significance owing to the fact that the majority of the SGWB is anticipated to emanate from a superposition of CBC events [5]. To elucidate the characteristics or nature of the SGWB, it is imperative to consider the properties of such events as described above [2].

The SGWB: An overview

The SGWB is a complex amalgamation of multiple sources of GWs that offer valuable insights into the evolution and history of astrophysical collisions over the universe's timespan [4]. Although numerous theorized sources, including cosmic strings, primordial black holes, etc, have been suggested to contribute to the SGWB, the vast majority of this background is expected to originate from a superposition of sources that are fully describable with parameterized models, CBCs, along with less predictable, unmodeled bursts such as core-collapse supernovae [4, 5]. This component of the SGWB is the astrophysical background, and is expected to be made up of the superposition of numerous GW events throughout the universe's history [4, 5]. A much smaller component of the SGWB consists of a cosmological background, including the GWs predicted to be formed immediately after the Big Bang through processes such as the preheating phase at the end of Cosmic Inflation, and GWs generated during inflation [11, 12, 13]. Other hypothesized sources include baryonic acoustic oscillations, or even further back with contributions from earlier phase transitions [4]. Although this portion of the SGWB is fainter, we note that its frequency lies beyond the detectable range of the ground-based GW detectors, which encompass a frequency of 20-5000 Hz [11, 12, 13], and some of the advanced GW experiments such as Laser Interferometer Space Antenna (LISA) or even the Pulsar Timing Array (PTA) [9]. Thus, this report focuses on the astrophysical component from CBCs.

The SGWB is expected to be stochastic in nature (although scientists are beginning to realize that it is only an approximation dependent on the detector sensitivity and may be resolvable in next-generation detectors) with a source distribution assumed to be isotropic, as well as being randomly distributed across the observable universe [10]. An alternate anisotropy, that of a background centered around local galaxy superclusters, is also discussed later in this report.

The SGWB: Expected detection signature

The signal of the SGWB is currently indistinguishable from detector noise arising out of ground systems such as LIGO. This is shown in Figure 2 below, wherein the stochastic signal is enclosed within a higher amplitude noise. Cross correlation between detectors is needed to extract useful parameter information on the SGWB. However, the same signal, in more sensitive next-generation detectors, will be distinguishable from noise. Figure 2 [10] depicts a prototype of the stochastic signal anticipated to resemble the SGWB.

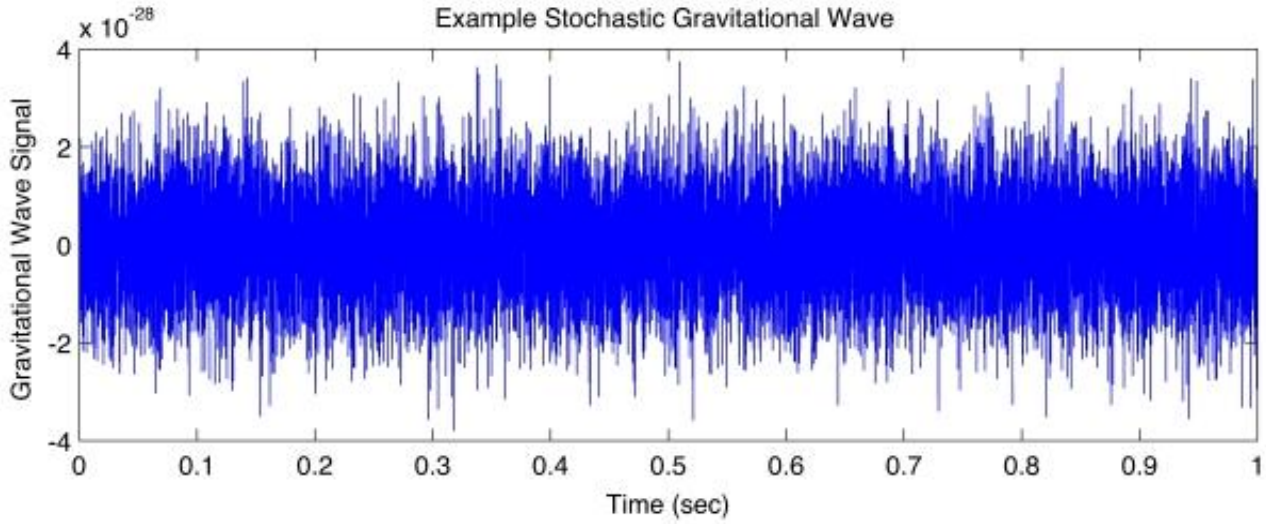

Figure 2: An example of a signal from a stochastic GW source. The signal is roughly uniform in amplitude and frequency in time, and is very faint [10]. The amplitude of the detector noise is up to six times higher than the amplitude of the signal.

Source: LIGO Scientific Collaboration [10]

While Figure 2 above shows the overall expected signal that would be observed in the event of an SGWB detection, we can also look at specific signal parameters over an entire frequency band to extract useful information on the SGWB [6, 7]. The variable we focus on is the energy density of the SGWB or the term Ω_{GW}, and we plot this value over a range of frequencies, since the SGWB covers a vast frequency range [6, 7]. The energy density of the SGWB provides an insight into the distribution of CBC events responsible for producing the background [6, 7]. While a greater deep dive into Ω_{GW} will be covered in later sections, as well as the various dependencies the term has on the frequency domain, merger mass distribution, and red shift, we introduce a brief overview here [6, 7, 19]. Notably, as shown in Figure 3 below, we can not only predict Ω_{GW} of the SGWB resulting from CBCs for various frequencies, but we can also show how with each subsequent observing run of the LVK network, the energy density values that the LVK can reach gets closer to the predicted SGWB energy density [6, 7, 19]. Therefore, to aid in

future detection of an SGWB, and to constrain predictions on the energy density of the background, we focus on building models of $\Omega_{GW}(f)$ from the SGWB [6, 7, 19]. Again, a more detailed analysis of the various parameters that affect Ω_{GW}, as well as the various methods to produce simulated energy densities will be discussed later [6, 7, 19].

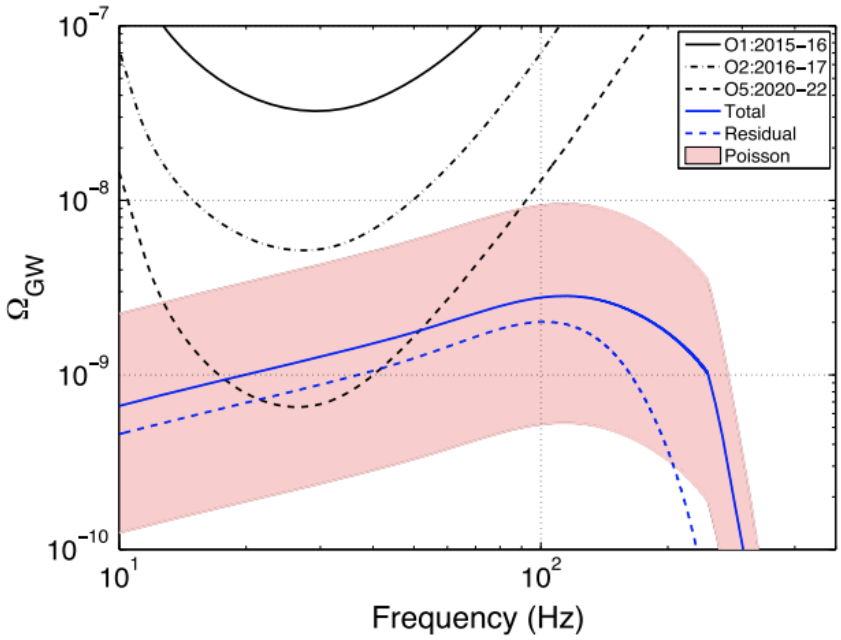

Figure 3: The energy density Ω_{GW} versus frequency for the total GWB corresponding to all CBC merger events shown in the blue line. The uncertainty in the merger rate, dominated by poisson error on the number of events detected by the IGWN, is also shown in pink giving the range of possible Ω_{GW} curves [6]. Also shown is an outdated prediction for the sensitivity of the IGWN to the SGWB in their first few observing runs. A more up to date impression of the energy densities each LVK observing run can reach is shown in later figures.

Source: GW150914: *Implications for the Stochastic Gravitational-Wave Background from Binary Black Holes,* B. P. Abbott et al, (LIGO Scientific Collaboration and Virgo Collaboration), *Phys. Rev. Lett.* 116, 131102, Published March 31, 2016, https://journals.aps.org/prl/abstract/10.1103/PhysRevLett.116.131102

While analyzing a simulated SGWB by looking at its energy density, we aim at studying the dependency of Ω_{GW} and the SGWB as a whole on merger rate, mass distribution, and the evolution of **these astrophysical parameters** with redshift. We expect the rough shape of the SGWB to be a broken power law (as shown in Figure 3 above) with a peak at a maximum energy density and a particular frequency value [6, 7, 19]. There are two distinct reasons for this turn-over: The most important is that the spectral energy density of individual CBC events $\frac{dE}{df_s}$ in the source frame peaks at merger and then falls off at higher source frequency f_s; and the higher the total mass of the CBC source, the lower the peak frequency: f_s^{peak} is proportional to $\frac{1}{M_s}$, where M is mass distribution. The second reason is that CBC sources at finite redshift produce red shifted spectral energy densities at the detector, such that the detector frequency = $\frac{f_s}{1+z}$. We

expect the merger rate to peak during (or after) ‘Cosmic Noon’, when the star formation rate of the universe was at its maximum, at a redshift of approximately 2 [16]. We also do not expect any mergers to occur before ‘Cosmic Dawn’ or when the first stars were born [16, 20]. The observed merger rate is in principle predictable under the assumption that mergers follow the birth of individual compact objects in binary systems, related to the star formation rate as a function of redshift. [6, 7, 19, 20].

Motivation: Constraining the astrophysical parameters of SGWB

GWs convey vital information on their sources, and likewise, the SGWB provides valuable insights into the underlying population of astrophysical sources that constitute it, including their mass distribution, the rate of formation of CBCs, and other parameters [5, 6]. Thus, by simulating SGWB with changing parameters, including amplitude, spectral shape, and angular distribution of sources, a novel window to understand the evolution of CBCs can open, targeting new, in-depth knowledge on how the mass distribution of compact binary systems and their sky location and redshift distribution impact the SGWB, which potentially reveal further insights into the astrophysical origins of GWs [14].

The primary motivation for our endeavor to compare the differing methods of simulating SGWBs is to further constrain the expected detection of such a background, and understand the new insights that can be gathered on the evolution of CBCs over cosmic time. Currently, due to relativistic numerical simulations estimating parameters of the SGWB, as well as new estimates generated by the LIGO, VIRGO, KAGRA (LVK) detectors, we have begun to constrain the limits of the SGWB [6], the expected signal to noise ratio (SNR) needed for detection, and the mean expected energy density of the background. The results can be summarized in Figure 4 below:

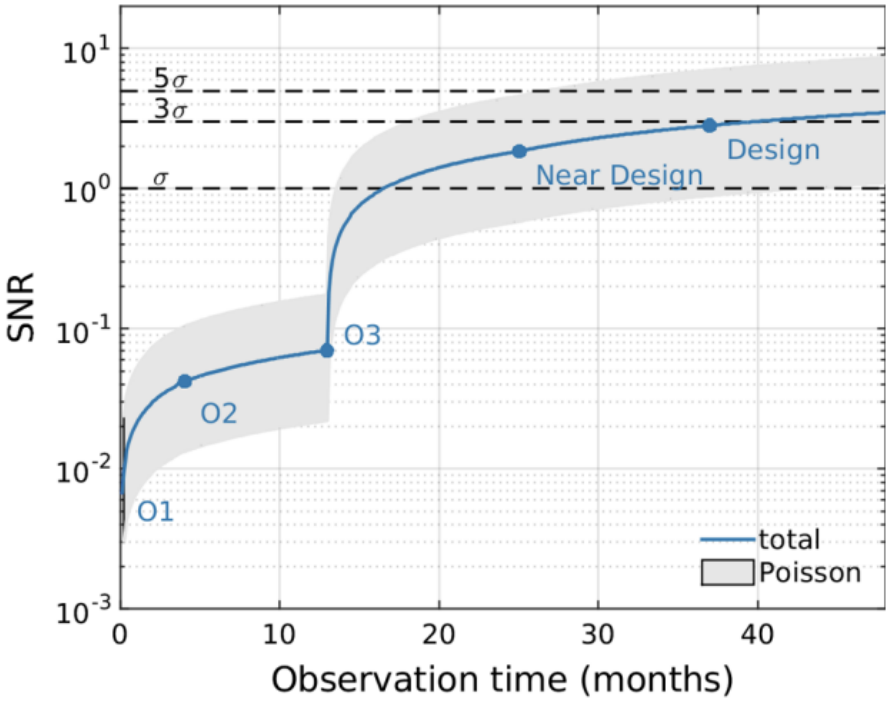

Figure 4: The image above shows the improvements in detector SNR (ratio of signal power to noise power or signal to noise ratio) [6, 19]. As measured SNR increases, the sensitivity level of the SGWB will also be reached by the LVK network [6, 19]. Therefore, as signal to noise ratio improves with subsequent observing runs, the sensitivity of LVK detectors improves over time, eventually resulting in a potential detection of the SGWB within a few years. The result of this research project, hence, contributes to further constraining and understanding the methodologies used to construct predictions of the SGWB, as well as decoding the range of possible predictions from simulation [6, 19].

Source: Fig 1 (right), GW170817: *Implications for the Stochastic Gravitational-Wave Background from Compact Binary Coalescences,* B. P. Abbott et al, (LIGO Scientific Collaboration and Virgo Collaboration), *Phys. Rev. Lett*, 120, 091101, Published February 28, 2018, https://journals.aps.org/prl/abstract/10.1103/PhysRevLett.120.091101

This research project aims at investigating the properties of the SGWB resulting from CBCs, with a focus on how different variables such as mass distributions, anisotropies, and redshift distributions impact the background signal. To accomplish this, the simulation techniques employed to model the SGWB are analyzed in detail, including how such models can be parametrized to account for different parameters [6, 7]. The theoretical framework for modeling the SGWB is developed, including understanding the power spectrum of strain fluctuations generated by the sources, along with a replication of the numerical simulations utilized to generate background signals for different scenarios [6, 7].

More specifically, the simulations are used to investigate the properties of the SGWB due to different mass distributions of CBCs. The impact of anisotropies in the distribution of CBC sources on the SGWB has also been studied. Additionally, this research project examines the impact of redshift evolution of these parameters on the SGWB due to CBCs. This includes investigating the potential for the SGWB to be affected by the evolution of the universe over time.

Overall, the goal of this research is to gain a deeper knowledge of the SGWB due to CBCs and the information it carries on the population of astrophysical sources that compose it. By studying how different variables impact the SGWB, we hope to develop a finer theoretical framework for modeling the background signal, which is crucial for interpreting future observations of the SGWB, and will aid in the overarching goal of gaining a better understanding of what to expect when the SGWB is finally detected.

Mathematical Background for SGWB

The SGWB is Gaussian (normally distributed), unpolarized compared to an individual source, and is expected to be isotropic in nature — or invariant with respect to sky location of the individual source [11]. This background can be fully characterized by the background energy density, and this spectrum can be expressed, as mentioned previously, by the term $\Omega_{GW}(f)$. This term allows for the calculation of the GW energy density within a frequency interval [11]. Specifically, $\Omega_{GW}(f)$ can be described by the equation below [11]:

$$\Omega_{GW}(f) = \frac{f}{\rho_c}\frac{d\rho_{GW}}{df} \quad (1)$$

Where $d\rho_{GW}$ is GW energy density, df the frequency interval, ρ_c the critical energy density needed to have a flat, non curved universe — defined as below:

$$\rho_c = \frac{3H_0^2c^2}{8\pi G} \quad (2)$$

Where c is the speed of light, G is Newton's gravitational constant, H_0 is Hubble constant, which we take from Planck satellite data as 67.4 km/s/Mpc [11].

Equation (1) for $\Omega_{GW}(f)$ derives a relationship between the energy density of the SGWB and the frequency content, thereby allowing us to understand the contribution of GWs for specific frequency intervals [11]. The frequency f that we measure in equation (1) above is of course the frequency measured by a detector. We take $f_s$as the frequency as observed in the source frame [11]. The term f_s is described by the equation $f = \frac{f_s}{1+z}$, wherein once again f is frequency in the detector frame [11]. We can decompose our equation (1) into another form below:

$$\Omega_{GW}(f) = \frac{f}{\rho_c}\frac{d\rho_{GW}}{df} = \frac{f}{\rho_c}\int_0^{10} \frac{R_m(z)}{(1+z)H(z)}\langle\frac{dE}{df_s}\rangle dz \quad (3)$$

In equation (3) [11], we still measure energy density of GWs within the frequency interval for the SGWB, but we now have $\Omega_{GW}(f)$ in terms of new parameters. $R_m(z)$ is the merger rate [11] in $\text{Gpc}^{-3}\text{yr}^{-1}$, which is explained in further detail later on. The parameter $H(z)$ is the Hubble expansion rate [11]. Notice that each parameter described (and the integral as a whole) is in terms of z, or the redshift. Typically, we assume that CBCs occur from a redshift of 20 (corresponding to the expected time in the universe's history when the first black holes are expected to form) till now (z=0) [11]. Thus, from equation (3), we have a preliminary link between the energy density of the SGWB, the redshift distribution that we are observing, as well as the mass distribution of CBCs, which the merger rate is dependent upon [11]. The overall aim of this research has been to evaluate equation (3) numerically. By creating simulations of the SGWB using mathematical models, such as the equation (3) above, we can manually adjust the merger rate through mass distribution, redshift distribution, etc. We can see the impact of variations in parameters to the energy density of the SGWB itself. The term $\Omega_{GW}(f)$ is the energy density of the SGWB, and is characterized by integrating the spectral energy density of the SGWB or the average of $\frac{dE}{df_s}$ [11]. It is a key quantity in the study of the SGWB, and is, therefore, used to calculate the energy density and SNR of the SGWB as it provides crucial insights into the properties of the GW sources that contribute to the SGWB background [11].

Computational methods

This study of the astrophysical SGWB relies on various tools, including numerical integration, specifically of the model used in equation 3, simulations of several gravitational wave events to construct estimates of $\langle\frac{dE}{df_s}\rangle$, coarse-grain example SGWBs to be generated, and dedicated Python packages, particularly pygwb — the latest released version — for all of the aforementioned gravitational wave science [20, 21]. Numerical integration techniques can be used to better understand the spectral energy density of the SGWB, and generate predictions on sensitivity ranges of various detector and mission operations to observe the presence of an SGWB [20, 21].

Therefore, such techniques remain a critical tool for the final stages for this research. The result of applying these methods on the energy density $\Omega_{GW}(f)$ — as defined by equation 3 — can be seen in Figure 5 below [8]. Note, unlike in figure 3, the contributions from BBH, BNS, NSBH merger events have been analyzed and plotted separately.

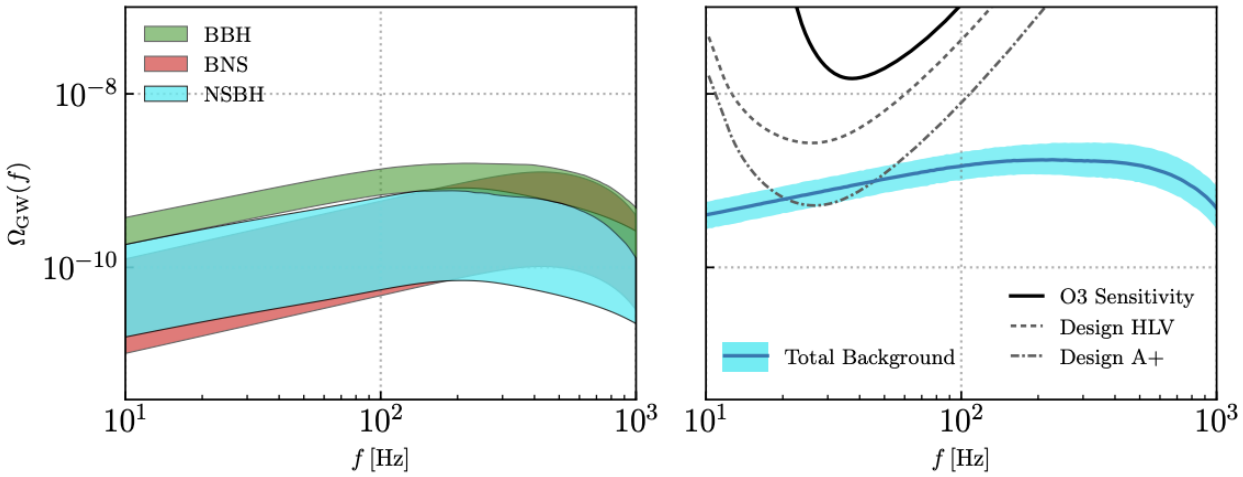

Figure 5: The image above shows the predictions of the SGWB due to CBCs as well as LVK detector sensitivity following Observation Run 3 [8]. Figure 5 (left) shows the expected contributions to the background from various astrophysical sources of gravitational waves, including binary black holes in green, binary neutron stars in red, and neutron star black hole mergers in blue [8]. Figure 5 (right) shows the sum of these three contributions (the total background) as the thin solid black line, with merger rate uncertainty shown as the blue band. It also shows the predicted detector sensitivity to $\Omega_{GW}(f)$ for present and near future versions of the LIGO detectors.

shows the intersection between detector sensitivity and required parameters needed to reach the SGWB detection sensitivity [8]. A key part of this research includes understanding the appropriate uncertainty in merger rate and mass distribution for each source of the CBC SGWB.

Source: *The population of merging compact binaries inferred using gravitational waves through*, GWTC-3, B. P. Abbott et al, (LIGO Scientific Collaboration and Virgo Collaboration), February 23, 2022, https://arxiv.org/abs/2111.03634, section X and Fig 23.

The other key tools that have been used during this research are simulations provided by Python packages for gravitational wave science, particularly pygwb [12]. Through simulations and coding, the project aims at utilizing different parameters and approximations for both mass distributions and redshift distributions in my research, apply statistical techniques to prototype SGWBs generated, study SNRs required to probe such backgrounds, etc.

Summary of objectives
The main objectives of this research are:

1. Reproducing and comparing the estimates of the CBC merger rate and the SGWB from [6] and [7], which are based on different numerical methods, including simple simulations of individual events and numerical evaluation of analytical expressions for the SGWB.
2. Investigating the degree to which these estimates agree with each other and the implications of any discrepancies.
3. Studying the dependence of these estimates on uncertainties in the merger rate as a function of mass, redshift distributions of the sources, and potential anisotropies in overall source distribution.
4. Assessing the impact of these uncertainties on any potential constraints that could be applied to the SGWB, including the energy density of the SGWB, contributions from different mass ranges of CBCs per frequency band, etc.

Final report

Description of both methods

Let us calculate and graph $\Omega_{GW}(f)$ over frequency as in [7]. To do this, we have followed the method utilized by Callister to simulate the background [20]. We start by revisiting equation 3 derived in the background section to provide an overview of the $\Omega_{GW}(f)$ calculation applicable to both the Callister and Regimbau methods [11]. This equation shows how the calculation of $\Omega_{GW}(f)$ or the background energy density of the SGWB depends on $R_m(z)$ or the merger rate, f_s or frequency in source frame, and f or frequency in detector frame, where $f = \frac{f_s}{1+z}$, z being redshift of source [11]. $\Omega_{GW}(f)$ is characterized by integrating the average spectral energy density of the ensemble of sources that make up the SGWB, $\langle\frac{dE}{df_s}\rangle$, and allows for the calculation of the GW energy density within a frequency interval [11]. Other important terms include $H(z)$ or the Hubble expansion rate, and ρ_c or the critical energy density needed to have a flat, uncurved Universe [11].

$$\Omega_{GW}(f) = \frac{f}{\rho_c}\frac{d\rho_{GW}}{df} = \frac{f}{\rho_c}\int_0^{10} \frac{R_m(z)}{(1+z)H(z)}\langle\frac{dE}{df_s}\rangle dz \quad (3)$$

This is the expression that both the Callister and Regimbau methods attempt to calculate. We can further decompose this equation by noting that $\frac{dE}{df_s}$ or the population averaged energy spectrum can be described as follows [17]:

$$\langle\frac{dE}{df_s}\rangle = \int dm_1 dm_2 \frac{dE}{df}(m_1, m_2, f(1+z))p(m_1, m_2) \quad (4)$$

Here, m_1, m_2 represent the masses of the two merging objects, $\frac{dE}{df}$ represents the spectral energy density of a GW from a single source using a simple model. And $p(m_1, m_2)$ represents their population probability distribution, dependent on their respective mass [17]. We can also break down the merger rate distribution describing it as an integral over a time delay distribution as described below [17]:

$$R_m(z) = \int dt_d R_*(z_f(z, t_d))F(Z < Z_c, z_f(z, t_d))p(t_d) \quad (5)$$

Thus, we see that the merger rate depends upon the time delay distribution $p(t_d)$, redshift values z, depending on frequency, the critical redshift or z_f and Z_c, as well as the formation redshift at the critical redshift or $F(Z < Z_c, z_f(z, t_d))$ and R_* or star formation rate [17]. Since we currently do not have exact limits on the time delay distribution, we fix $R_m(z)$ at z = 0.2 with LIGO data (Table IV of [8]), and use the crude model from section VI.D and figure 13 of [8] for the redshift

dependence.We decomposed both $R_m(z)$ and $\langle\frac{dE}{df_s}\rangle$, so we can start reproducing the method utilized for calculating and plotting $\Omega_{GW}(f)$ as used in [7, 17]. This process is the same as used in acquiring Figure 5 of [7] and a guide for following the path to calculating and graphing $\Omega_{GW}(f)$, which can be found in [17].

Method of summing over a grid of astrophysical model parameters

To give a brief overview of the Callister process, which is described in [17, 20] and the final result of which is represented in [7], we create a grid of (m_1, m_2) data values, and of frequency and redshift values, respectively [17, 20]. We can then precompute the spectral energy density for each combination of mass values, redshift of each source, and frequency of each signal [17, 20]. Thereafter, for a given mass distribution, we can calculate the probabilities of that distribution over the mass grid [17, 20]. Next, we aim to get a precomputed grid of binary formation rates (or rate of formation of CBC systems dependent on system mass) using an assumed star formation rate R_* [17, 20]. This grid is a function of merger redshift as well as time difference between binary system formation and merger or time delay [17, 20]. We can also get a probability distribution of time delay between source formation and merger, as inspiral times in such CBC systems are dependent on masses of the two objects in question [17, 20]. Much more importantly, they depend on the initial binary separation at formation, which is entirely unknown. To simplify the process further from here, we can get a merger rate of compact binaries from matrix multiplying our array of formation rates by a probability distribution of delay times [17, 20]. This is an intuitive explanation of the process of getting the pre computed grid of binary formation rates, as once again, we are uncertain about the actual time delay distribution and are unsure if mergers follow the formation of binaries as capture-based mergers can occur, where two initially non orbiting black holes capture each other to form a binary which may eventually merge [17].

Now, for actually encoding $\Omega_{GW}(f)$ through the Callister method, we can summarize the above by the following steps [20]: We first define a local merger rate and mass distribution, set up the $\Omega_{GW}(f)$ object, and then reweight it according to the mass distribution in order to integrate over the range of possible object masses [20]. We then compute $\Omega_{GW}(f)$ through a function taking into account mass distribution, local merger rate, evolution of merger rate with redshift, and frequency range over which we define $\Omega_{GW}(f)$ [20]. Overall, we calculate population averaged energy spectrum, $\langle\frac{dE}{df_s}\rangle$, over the entire frequency range to get $\Omega_{GW}(f)$ [17, 20]. Thus, we numerically evaluate equation (3) by gridding over parameter space, as can be shown below in the calculation of $\Omega_{GW}(f)$ by the following matrix product expression [17, 20]:

$$\Omega_{GW}(f) = \frac{f}{\rho_c}\frac{d\rho_{GW}}{df} = \frac{f}{\rho_c}\int \frac{R_m(z)}{(1+z)H(z)}\langle\frac{dE}{df_s}\rangle dz = \frac{f}{\rho_c}\sum_z \left\{\frac{R_m(z)}{(1+z)H(z)}\right\}_z \left\{\langle\frac{dE}{df}\rangle\right\}_{f,z} \quad (6)$$

Where $\left\{\langle\frac{dE}{df}\rangle\right\}_{f,z}$ is the population averaged energy spectrum dependent on frequency and redshift, and the curly brackets represent a matrix multiplication between the aforementioned grids we created [17]. Therefore, the energy density, $\Omega_{GW}(f)$, of the SGWB, as measured by a stochastic search, is described by a weighted integral over the CBC merger history over the universe's evolution and is sensitive to the totality of past mergers [17]. We can tune the minimum and maximum values of masses for neutron star binary mergers and black hole binary mergers with an assumed merger rate to arrive at plots of $\Omega_{GW}(f)$ over time, as shown in Figure 6 below [17,

20]. We have given a mass distribution for each of the object pairs in the simulated mergers that make up this modeled SGWB, each distribution having a maximum and minimum mass. This is because, to reiterate, the SGWB is a superposition of GWs from CBCs of pairs of merging objects.

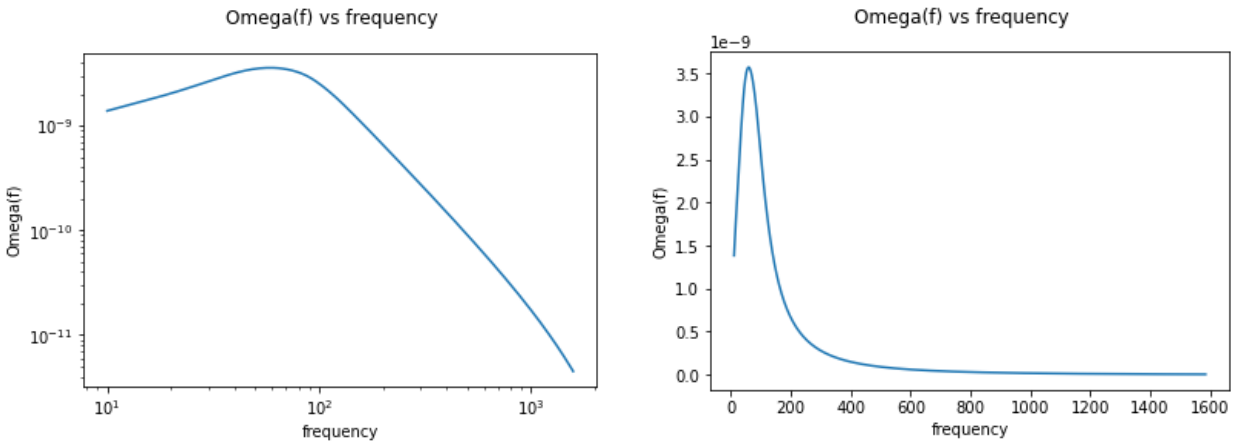

Figure 6: For the above plots (linear plot on right, logarithmic on left) we have taken a minimum mass of first merging object, m1_min = 2.5 solar masses, and a maximum mass of first merging object, m1_max = 100 solar masses, a minimum mass of second merging object m2_min = 1.5 solar masses and a maximum mass of second merging object of 100 solar masses [17, 20]. The mass distributions themselves were power laws. Note, the peak in the energy density is in the hundreds of Hz, and the fact that $\Omega_{GW}(f)$ is a broken power law distribution, is reflected as predicted. Thus, we have plotted the energy density of a simulated SGWB [17, 20].

Source: Image generated by the author, but the methodology used can be found through [7, 17, 20].

We can also do a test to see if the SGWB plot is in reality the same as we expected [20]. In particular, we can test the prediction that if we decrease the mass distribution by decreasing the maximum mass value in the merger, we should see the graph shift to higher frequencies. Figure 7 below shows exactly this [20].

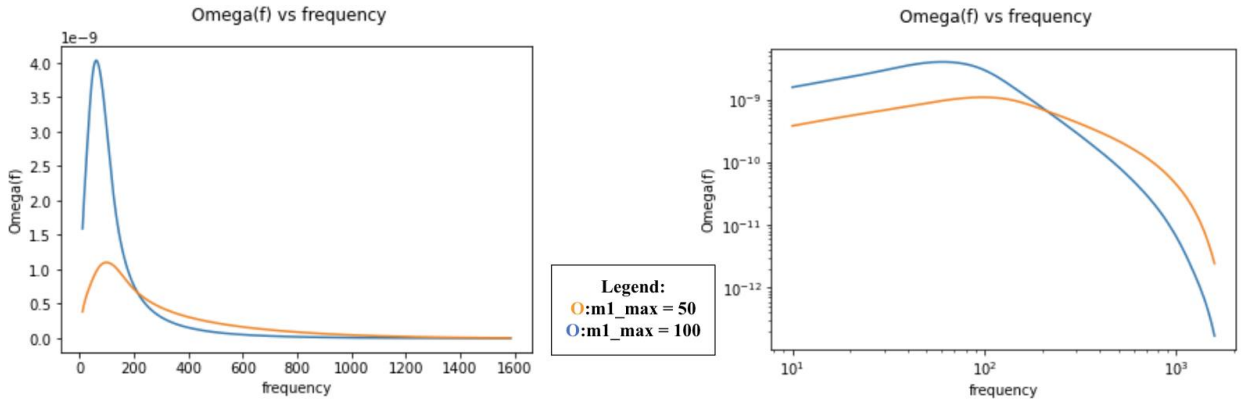

Figure 7: Here, we use the Callister method to create plots in both linear scale (left) and logarithmic scale (right) for different mass distributions [20]. On the orange plots we see a mass distribution with a minimum of 5 solar masses, maximum of 50 solar masses for the mass of one merging object. On the blue we see plots for a minimum of 5 solar masses, maximum of 100 solar masses for the mass of one merging object [20]. We can see that the peak of the 100-solar-mass maximum plot is shifted to the lower frequencies compared to the 50-solar-mass maximum plot (clearer on the log scale plot) which is exactly what we expect when we simulate higher mass distributions [20]. In both cases we have a 1:1 mass ratio between merging objects, so m1_mass = m2_mass [20].

Source: Image generated by author, but the methodology used can be found through [7, 17, 20].

We can repeat the plots shown in figure 7 but for a greater variation in maximum mass of the mass distribution, again we keep a 1:1 mass ratio between merging objects, and keep a constant minimum mass m1_min = m2_min = 5 solar masses, but we vary m1_max = m2_max as shown in Figure 8 below [20]:

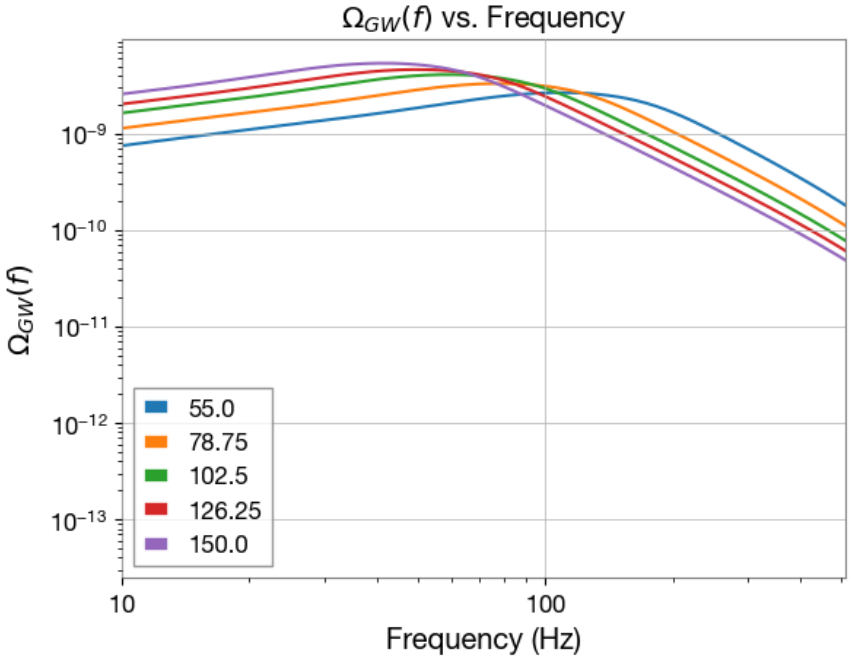

Figure 8: Here we see the application of the Callister method for a series of different mass distributions with m1 distribution = m2 distribution, both being power law distributions, but different maximum masses (as shown in the legend), where m1_max = m2_max= 55, 78.75, etc [20]. As can be seen, as mass distribution increases by having greater maximum masses, the curve shifts to lower frequencies [20].

Source: Image generated by the author, but the methodology used can be found through [7, 17, 20].

Thus, the Callister method creates spectra as per our predictions. If we continue to keep the maximum mass of both merging objects equal to one another (for one-to-one ratio of mass for the merging objects), and vary the maximum merging mass value, we can plot how frequency and $\Omega_{GW}(f)$ changes with mass distribution across several different maximum mass values [20]. The Callister method has m_1 and m_2 maximum values representing both merging objects [7, 17, 20]. If we keep increasing these values and repeating the graphs, and from there plot how frequency and $\Omega_{GW}(f)$ varies with maximum mass, we get Figure 9 as shown below [20]:

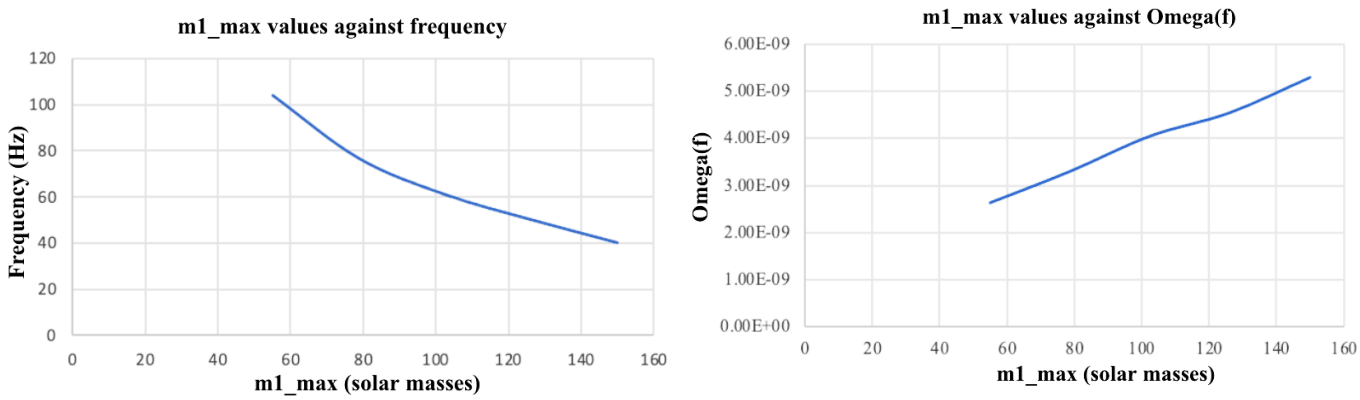

Figure 9: A linear scale plot of how peak frequency changes with mass distribution on the left and a linear scale plot for how peak $\Omega_{GW}(f)$ changes with mass distribution on the right [20]. In other words, we observe how the peak of the graphs from Figure 8 changes with the maximum value of the mass distribution for the merging masses with a 1:1 mass ratio between merging objects [20]. It is clear that with increasing mass distribution, by inclusion of higher and higher maximum merging masses as shown on the x axis, the frequency is shifted to lower and lower values, and $\Omega_{GW}(f)$ is shifted to higher and higher values [7, 17, 20]. The maximum merging mass represents the maximum mass expected for m_1 and m_2 in mergers [20].

Source: Image generated by the author, but the methodology used can be found through [7, 17, 20].

It should be noted that this result is dependent on several factors, especially if the local merger rate assumed in the Callister method remains constant in redshift [7, 17]. For Figure 9, we assume that the merger rate remains constant [7, 17, 20]. However, the mass distribution has been changed, thus leading to the plot shown above in Figure 9 [7, 17, 20]. However, more

refined plots will need to be generated to replicate the result shown in Figure 9, as it is still unclear whether or not we expect such a wide variation in frequency range from this particular variation in maximum mass distribution [7, 17, 20]. More simulations are needed to better understand how the merger rate function R_m also depends upon mass as an integral over mass distribution. We also understand that the Callister method uses a simple $\frac{dE}{df}$ proportional to $f^{-\frac{7}{3}}$, which we know to be incorrect. Therefore, there are still numerous refinements and changes that need to be made to this method.

If we take the local merger rate (or merger rate at our current redshift of 0), we can change this value to see how it impacts $\Omega_{GW}(f)$ across a frequency range. This result is shown in Figure 10 below [17, 20]. Note that for this analysis, we have chosen specific fixed merger rates to see how measurement uncertainties may affect the plots [17, 20].

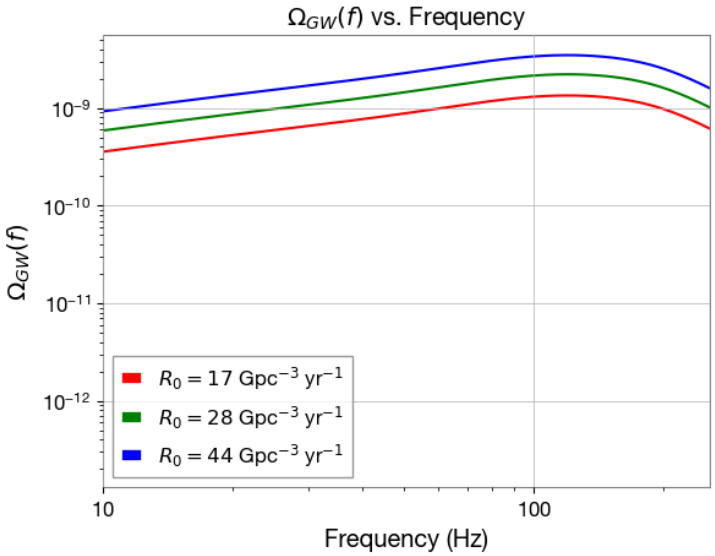

Figure 10: A plot of how $\Omega_{GW}(f)$ against frequency changes with different mean local merger rates. The graph is shifted to higher values of $\Omega_{GW}(f)$ when greater merger rates are applied — an expected outcome — as $\Omega_{GW}(f)$ represents the energy density of the SGWB. If the rate of mergers is higher, then the energy density of the SGWB is higher as well [7, 17, 20].

Source: Image generated by author, but the methodology used can be found through [7, 17, 20].

Method of summing over individual events

Now, we can also do the same calculation as described in [7,17] and plot for $\Omega_{GW}(f)$, but use a different method [18, 21] than the one used in [20]. This is the process as outlined in [6]. This method utilized by Regimbau, and later simplified and standardized by Renzini, is Monte-Carlo-based unlike the Callister method [18, 21]. The brief overview of this methodology is that it aims at using a Monte-Carlo sampling of individual injections of CBC events from an assumed population distribution distribution to build up $\Omega_{GW}(f)$ across a frequency range [18, 21].

$$\Omega_{GW}(f) \propto \frac{1}{T_{obs}} \sum_0^N \quad f^3 \frac{dE}{df} \tag{7}$$

As can be seen in equation (7), we are building up $\Omega_{GW}(f)$ from a number of simulated events or injections N drawn from a population characterized by $p(m_1, m_2)$ and $R_m(m_1, m_2, z)$ (c.f. Equations 3 and 4 above)

[18, 21]. As we can see, the greater the number of injections, the more accurate the curve will be. In other words, a list of CBCs is created with random parameters from a given set of astrophysical bilby priors (where bilby is the python package utilized), including prior probability of masses, luminosity distance, etc [18, 21]. Finally, the total injected $\Omega_{GW}(f)$ can be computed in the frequency domain [18]. The overall goal is to compute $\Omega_{GW}(f)$ through the injection of individual CBC events [18]. We can increase the number of injections, thereby resulting in a smoother curve, and then for each injection we can generate a parameter dictionary, a frequency domain waveform, orientation factor, and ultimately arrive at the final PSD of the signal, which is then added to the $\Omega_{GW}(f)$ spectrum [18, 21]. The injections are sampled via Monte-Carlo methods. Thus, we can again calculate $\Omega_{GW}(f)$ as shown in Figure 11 below [18, 21]:

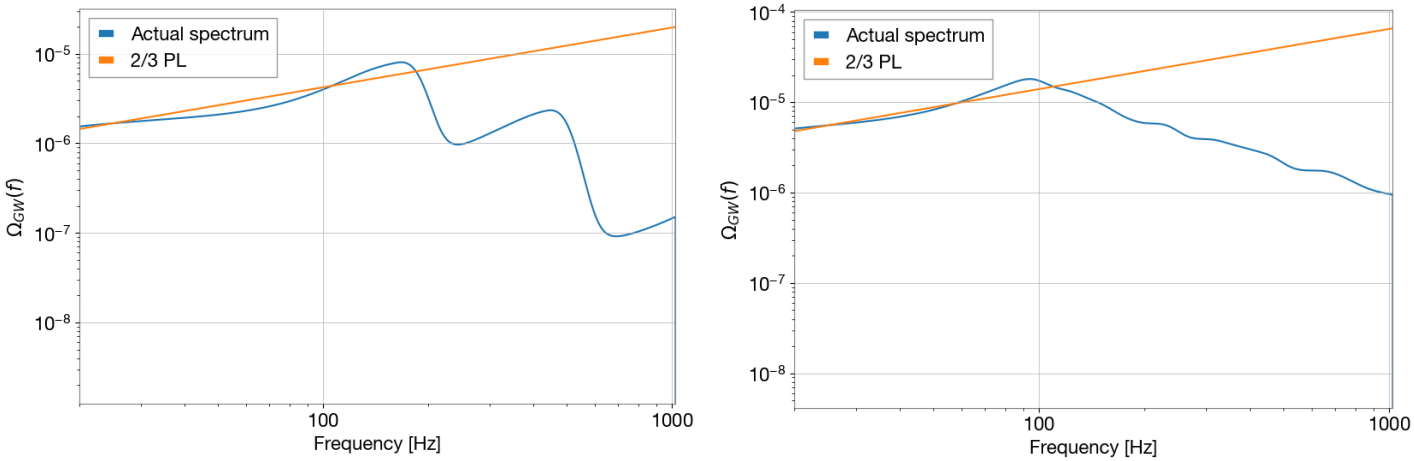

Figure 11: $\Omega_{GW}(f)$ over a frequency range compared to a power law of ⅔ [18]. The priors that we specify are the average ratio of the masses in CBCs, the average masses themselves, luminosity distance, and a host of other variables [18, 21]. If we set luminosity distance to a power law function with a minimum of 100 Mpc to 1000 Mpc, we can get the above Figure 8 (left and right) through an average mass ratio of 1.0, setting both priors for mass 1 and mass 2 to uniform distributions with a minimum of 1.5 and a maximum of 100 solar masses [18, 21]. Note that 10 injections were used to create the left figure and 100 injections were used to create the right figure [18, 21].

Source: Images generated by the author, but the methodology used can be found through [18, 21].

Therefore, to solve the issue of excess fluctuations in the graph, we can increase the number of injections, as shown in figure 11 above [18, 21]. This ensures that there are fewer fluctuations in the data at higher values of frequency [18, 21]. At lower injections, it becomes difficult to identify what peak is an aspect of the curve that can be smoothed out with more injections or

what is an actual feature of the $\Omega_{GW}(f)$ versus frequency relationship [21]. If we keep all values the same as in Figure 11 above, but increase the number of injections to 1000, we get Figure 12 below [18, 21]:

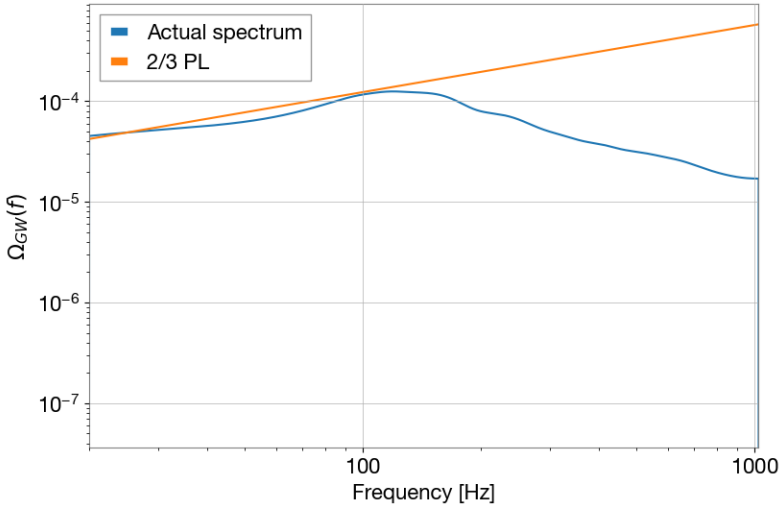

Figure 12: Using the same parameter priors in Figure 10, with 1000 injections, we can get a smoother curve, cementing the essentialness of using as many injections as possible when using the Regimbau method [18, 21]. Note, that each peak may correspond to some important contribution towards $\Omega_{GW}(f)$ [6]. Thus, a crucial aim for future research lies in analyzing the distribution of peaks with different parameters or prior inputs [18, 21].

Source: Image generated by the author, but the methodology used can be found through [6, 18, 21].

In the Callister method, all $\Omega_{GW}(f)$ values are in an order of magnitude that is 10^{-10} , while in the Regimbau method, $\Omega_{GW}(f)$ values can be between 10^{-4} to 10^{-8}. We can still see the difference in $\Omega_{GW}(f)$ values by normalizing all inputs — and removing the neutron star contribution from the Callister method — by setting both m_1 and m_2 values to be a minimum of 5 and a maximum of 50 solar masses [20, 21]. We also ensure that both m_1 and m_2 values in the Regimbau method can be described by a normal distribution with a minimum of 5 and a maximum of 50 solar masses [20, 21]. The results of this comparison are shown in Figure 13 [20, 21] below:

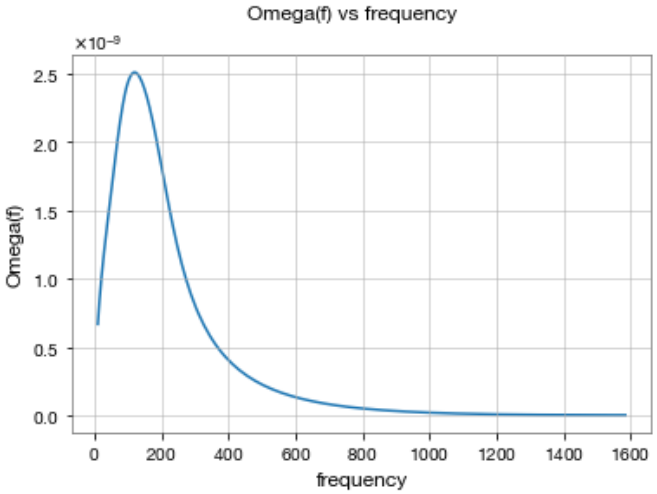

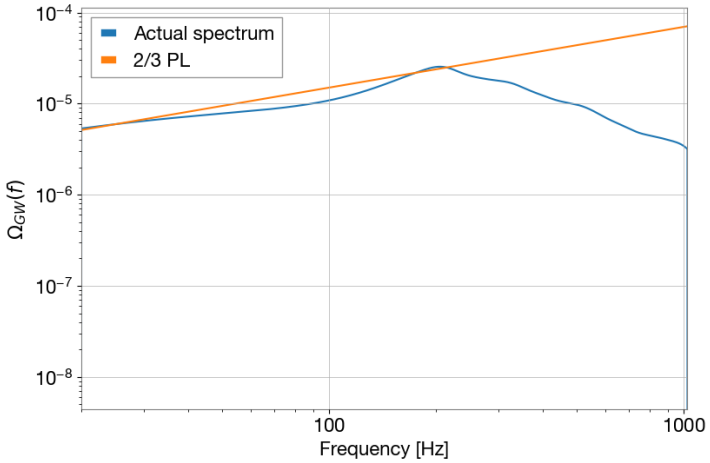

Figure 13: The result of the above constraints for both the Callister method (left) and the Regimbau method (right) [20, 21]. As can be seen, while both methods peak at a similar frequency (somewhere in the range of 2×10^2Hz, their peak values, and therefore the entire graphs, fall on entirely different frequency ranges. While the Callister method typically results in peak $\Omega_{GW}(f)$ values in a range from 10^{-8} to 10^{-9} Hz, the Regimbau method typically results in peak $\Omega_{GW}(f)$ values between 10^{-4} to 10^{-8} [20, 21].

Source: Images generated by the author.

This discrepancy is a result of the fact that observation time and number of injections are related in the Regimbau method, when in fact they should be separate from each other [17, 18]. When we look back at equation (7), we can modify it to get a relationship between observation time and number of injections [17, 18].

$$\Omega_{GW}(f) \propto \frac{1}{T_{obs}} \sum_0^N f^3 \frac{dE}{df} \quad (8)$$

$$T_{obs} \propto \sum_0^N f^3 \frac{dE}{df} \quad (9)$$

However, the way we have done this is that we have forgot to normalize the equation as there is ultimately no physical relationship between $\Omega_{GW}(f)$ and number of injections, which is to say that energy density of background should remain constant regardless of injections, so we needed to use $\frac{1}{N} \sum_0^N f^3 \frac{dE}{df}$ to normalize equation (9), where again, N is the number of events [17, 18]. Thus, the overall idea behind the relation between observation time and number of injections is that although these can be described as such that injection number is proportional to observation time, we can normalize both sides by the number of injections to remove this proportionality, as again, physically, these quantities should be independent of $\Omega_{GW}(f)$ [17, 18]. We expect that the error in the implementation of the Regimbau method, wherein it gives a much higher than expected value, is due to this normalization error, but of course, further research is needed at this time [17, 18]. The Callister method is not reliant on injections so does not face the same issue as with the Regimbau method, thereby currently giving more accurate estimates on $\Omega_{GW}(f)$ [17, 18].

However, because we still show the proportionality between observation time and injection number, as with equation (9), we can still try calculating the number of injections based on observation time to try and get the Regimbau method to match the results of the Callister method [17, 18]. This helps to validate both methods, check that both methods are capable of consistently providing useful and expected outputs, and ultimately leads to more effective methods of combining the methods, as will be detailed later [17, 18]. We can fine tune for certain values of luminosity distance, set a common distribution/observation time of one year, and calculate injections from there [17, 18]. With a common mass distribution of 5 to 50 solar masses, we have the comparison plot in Figure 14 below [17, 18]:

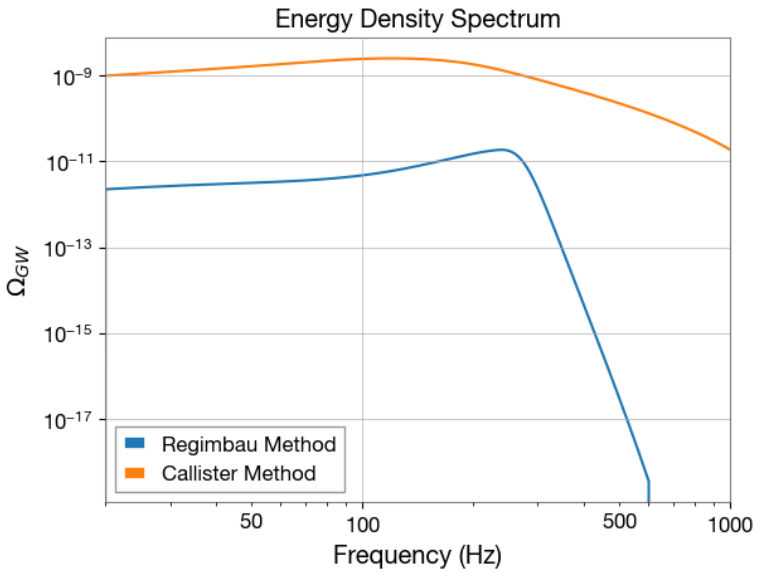

Figure 14: By calculating injections roughly based on a common observation time with the Callister method, we are able to adjust the parameters in the Regimbau method to roughly agree within the same order of magnitude as the Callister method. It should be noted, however, that while the Regimbau method in this case uses a uniform mass distribution — and this can be changed to a power law, broken power law, etc — the Callister method is inbuilt with a power law distribution. Even so, we can still see better agreement between the two methods [17, 18].

Source: Images generated by the author.

We can continue to adjust the observation time in the Callister and Regimbau methods, such that the number of injections matches the appropriate observation time. The result for both m_1 and m_2 with a log distribution of between 5 and 50 solar masses and a redshift distribution from our current redshift of 0 to a redshift of 2 (given by a power law) is shown in Figure 15 [17, 18] below:

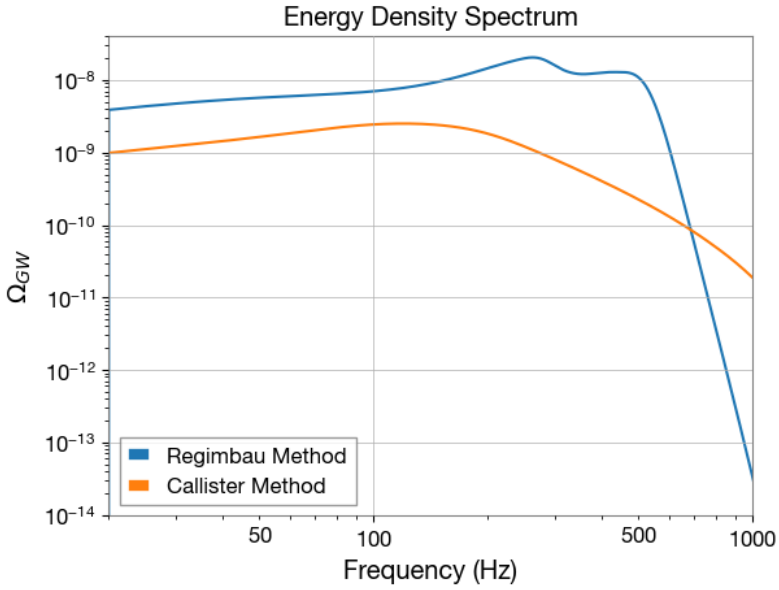

Figure 15: Another attempt is to adjust the observation time for both methods and match the appropriate number of injections to be utilized for the Regimbau method. The two methods now provide results that are close to the same magnitude, suggesting success for this methodology. Instead of using luminosity distance to tune the injections, we use a redshift parameter [17, 18].

Source: Images generated by the author.

We can also try other pathways to combine the Regimbau and Callister methods. Whilst the Callister method is grid based, as described in equation (6), with the change in probability over the mass distribution being multiplied by a calculated Jacobian, we can instead use bilby priors for specifying prior probability of both merging masses 1 and 2 [17, 18]. In other words, we are using the priors from the Regimbau method to calculate the probabilities in the Callister method [17, 18]. The final result of doing this is specified in Figure 16 below:

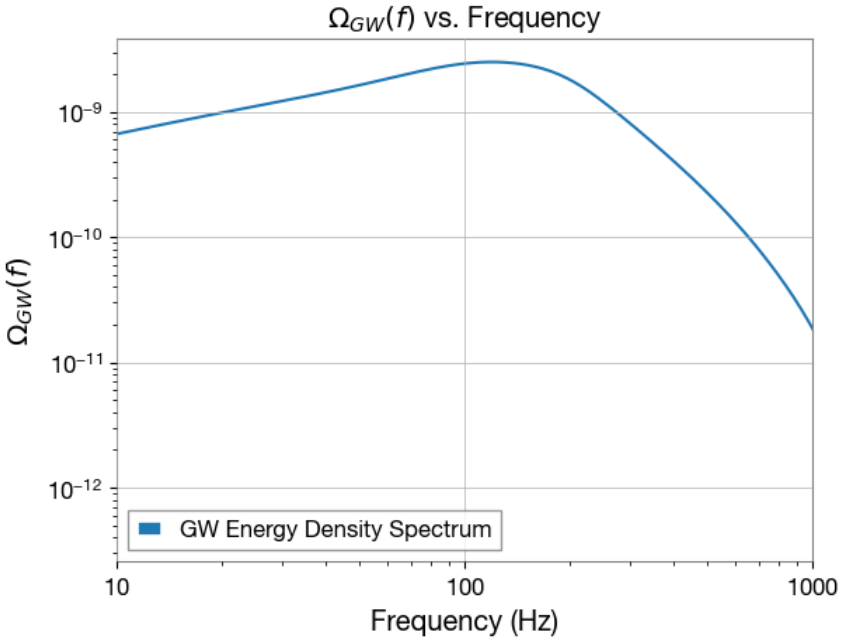

Figure 16: The final $\Omega_{GW}(f)$ against frequency plot resulting from using probability priors from the Regimbau method within the Callister method. As can be seen, calculating probability this way still overall results in a peak $\Omega_{GW}(f)$ of around 10^{-8} as is appropriate [17, 18].

Source: Images generated by the author.

Thus, we have managed to temporarily ensure that the two methods agree with one another to at least an order of magnitude, as well as combined the two methods in terms of probabilities and still achieved an accurate result. An attempt still needs to be made to fully characterize the injections used in the Regimbau method in terms of the Callister method and observation time. An attempt has also been made on this for the specific observation time of one year, one day, and so on [17, 18].

Next steps and conclusion

As per the section on main objectives, throughout the first part of our research, we have reproduced estimates of energy density of the SGWB from [6] and [7] using corresponding methods in [18] and [17] respectively and corresponding tools in [20] and [21] respectively. By repeating the simulations with different mass distributions and merger rate values, we have quantified the dependence of the estimates on uncertainties in merger rate as a function of mass [17, 18]. We have looked at the degree to which these estimates agree with each other, calculated specific observation times and instances of reasonable agreement between these methods, as well as impacts of uncertainties on potential constraints that can be applied to the SGWB's energy density [17, 18]. We have begun inputting priors into the Callister method in the same way that they are utilized in the Regimbau method to allow for a greater comparison between the two methodologies [17, 18] and the two pathway tools [20, 21] .

Our next main goals are to continue generating $\Omega_{GW}(f)$ plots for both the Regimbau and Callister methods, understand the parameter distribution that leads to each plot result, such as merger rate, energy density, frequency etc, and understand how these parameters evolve with differences in mass and redshift distribution [17, 18]. Recent work has been conducted as part of this research on varying the mass distribution of mergers — each represented by a single mass of the merging pair — for different redshift values to see that as we scale mass distribution with redshift, the cut-off value for mass distribution gets larger and larger. Provided are some example variations in mass distribution scaled to be less than 100 solar masses as a starting model.

We define the cut-off as follows: If we plot the change in mass merger rate with redshift against mass values as a power law, we see there is a point where the change in gradient with change in mass is negligible. The mass value that this occurs at, is the cut-off of the mass values. We plot this graph for redshifts from 0 (our reference frame) to a redshift of 2 as shown in Figure 17 below. We see that the cut-off values for mass distributions increase with redshift.

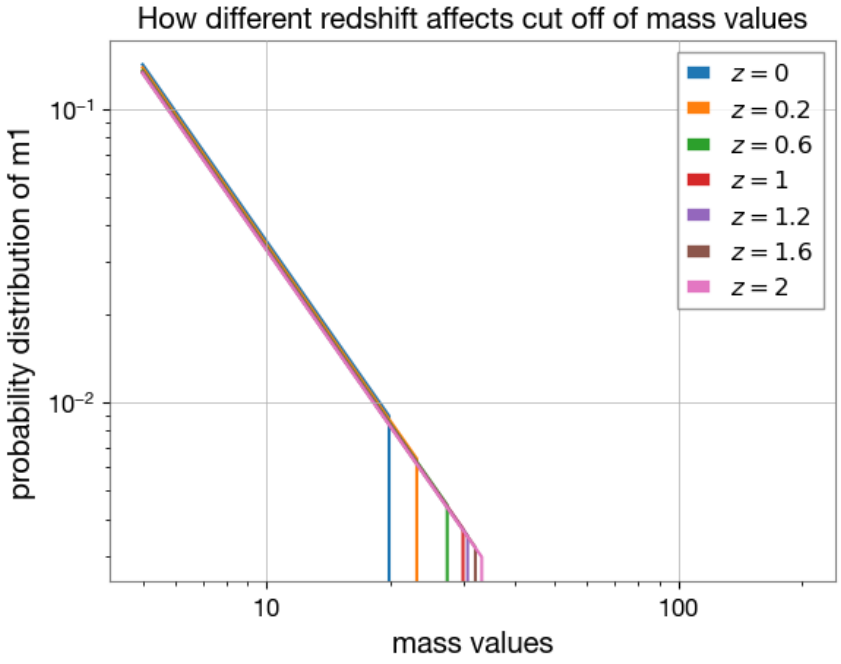

Figure 17: A graph showing how different redshifts affect cut-off values of mass distribution — the point wherein change in mass merger rate for a given change is negligible. This cut-off occurs at higher mass values for higher redshifts.

Source: Images generated by the author.

The purpose of this cut off value analysis is to better look at the mass distribution of mergers. We expect the mass distribution to look somewhat like a 'Power law + Peak distribution' given by the following equation.

$$p(m_1) = m_1^{-\alpha} + ce^{-(m_1 - m_1^*)^2/\delta_{m_1}^2} \quad (10)$$

As can be seen in equation (10), the mass distribution $p(m_1)$ can be described as the sum of a power law $m_1^{-\alpha}$, with $-\alpha$ being the slope of this power law, and a peak formula that we will explore in later research. Instead of looking at the cut off value of this formula, we can also scale the slope of the mass distribution with different redshift values. Therefore, we can scale the α values, which is given by the following equation.

$$\alpha = \alpha_0 + \alpha^* z \quad (11)$$

We scale both the initial α_0 as well as α^* (or the change in alpha with the change in redshift) for different redshift values. The result of doing this is shown in Figure 18 below:

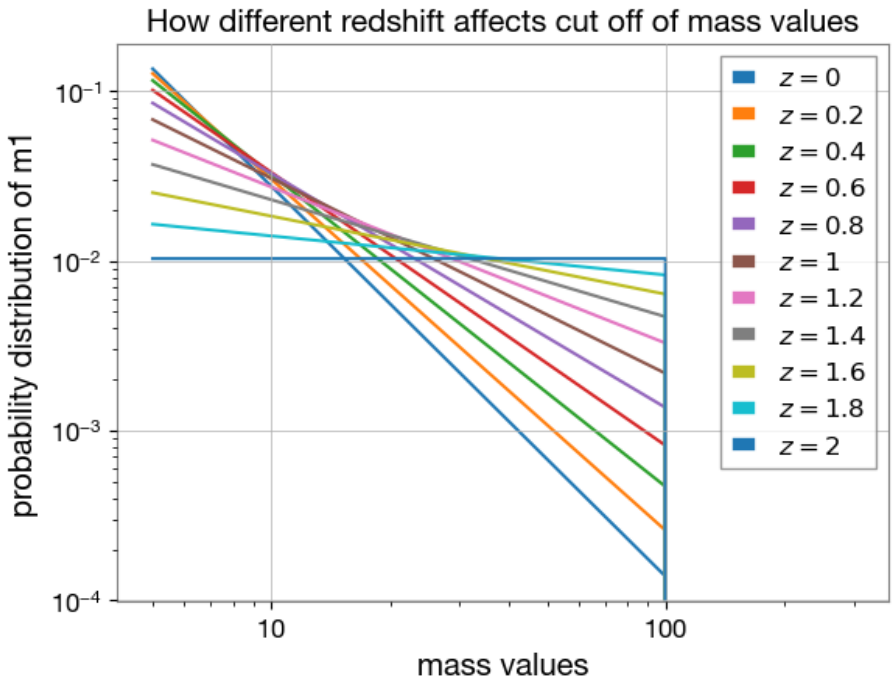

Figure 18: A graph showing how different redshifts affect slope alpha values of mass distribution. Here we fix the cut off mass at 100 solar masses, and ensure α^* is half of α_0 so that the slope of the graph would be 0 at a redshift of 2, which we easily observe, showing we have achieved the expected correct results.

Source: Images generated by the author.

Further work will need to be completed on breaking down the equations defining the change in merger rate with respect to peak merger mass, the overall probability distribution given particular mass distributions. More research will need to be done on how all of equation (10) — the entire power law + peak distribution — scales with redshift, as well as substituting this new mass distribution into the Callister and Regimbau methods [17, 18, 20, 21].

In any case, the overall goal of this project will be to continue investigating the relationship between various parameters and hyperparameters with changes in mass distribution and redshift distribution. Moreover, a longer-term goal will be to actually use the data collected on SGWB [15]. Overall, the next steps will also be to repeat the same analysis of $\Omega_{GW}(f)$, but measure it as it varies with redshift distribution, thereby looking at the impacts of potential anisotropies.

Acknowledgements
California Institute of Technology (Caltech), USA
The Laser Interferometer Gravitational-Wave Observatory (LIGO), Caltech and Hanford, USA
The LIGO SURF program, Caltech, USA
National Science Foundation (NSF)

Bibliography

[1] *LIGO, VIRGO And KAGRA Observing Run Plans*, IGWN, accessed May 2023, https://observing.docs.ligo.org/plan/

[2] *Gravitational Waves from Compact Binary Mergers seen by LIGO and Virgo*, Alan J Weinstein LIGO Laboratory, Caltech for the LIGO and Virgo Collaborations LIGO-Virgo Open Data Workshop, May 27, 2020, https://dcc.ligo.org/public/0168/G2000797/001/Weinstein_CBCs_GWOSC_ODW_20200527.pdf

[3] *Gravitational-wave Transient Catalog (GWTC)*, LVK Collaboration, https://www.gw-openscience.org/eventapi/html/GWTC/

[4] *Stochastic Gravitational-Wave Backgrounds: Current Detection Efforts and Future Prospects*, Renzini, A.I., Goncharov, B., Jenkins, A.C., Meyers, P.M., *Galaxies 2022*, 14 February 2022, https://www.mdpi.com/2075-4434/10/1/34

[5] *Upper limits on the isotropic gravitational-wave background from Advanced LIGO and Advanced Virgo's third observing run*, R. Abbott et al, (LIGO Scientific Collaboration, Virgo Collaboration, and KAGRA Collaboration), *Phys. Rev.* D 104, 022004, Published July 23, 2021, https://journals.aps.org/prd/abstract/10.1103/PhysRevD.104.022004

[6] GW150914: GW150914: *Implications for the Stochastic Gravitational-Wave Background from Binary Black Holes*, B. P. Abbott et al, (LIGO Scientific Collaboration and Virgo Collaboration), *Phys. Rev. Lett.* 116, 131102, Published March 31, 2016, https://journals.aps.org/prl/abstract/10.1103/PhysRevLett.116.131102;

[7] *Upper limits on the isotropic gravitational-wave background from Advanced LIGO and Advanced Virgo's third observing run,* R. Abbott et al, (LIGO Scientific Collaboration, Virgo Collaboration, and KAGRA Collaboration), *Phys. Rev. D,* 104, 022004, Published July 23, 2021, https://journals.aps.org/prd/abstract/10.1103/PhysRevD.104.022004, section V.A

[8] *The population of merging compact binaries inferred using gravitational waves through*, GWTC-3, B. P. Abbott et al, (LIGO Scientific Collaboration and Virgo Collaboration), February 23, 2022, https://arxiv.org/abs/2111.03634, section X and Fig 23.

[9] *The stochastic gravitational-wave background from massive black hole binary systems: implications for observations with Pulsar Timing Arrays*, *Monthly Notices of the Royal Astronomical Society*, A. Sesana, A. Vecchio, C. N. Colacino, Volume 390, Issue 1, October 2008, Pages 192-209, https://doi.org/10.1111/j.1365-2966.2008.13682.x

[10] *Introduction To Ligo & Gravitational Waves, Stochastic Gravitational Waves*, LVK Collaboration, https://www.ligo.org/science/GW-Stochastic.php, accessed May 2023

[11] *Impact of a Midband Gravitational Wave Experiment On Detectability of Cosmological Stochastic Gravitational Wave Backgrounds*, Barry C. Barish, Simeon Bird, and Yanou Cui, 16 June 2021, https://arxiv.org/pdf/2012.07874.pdf

[12] *pygwb documentation*, Copyright 2022, Arianna Renzini, Sylvia Biscoveanu, Shivaraj Khandasamy, Kamiel Janssens, Max Lalleman, Katarina Martinovic, Andrew Matas, Patrick Meyers, Alba Romero, Colm Talbot, Leo Tsukada, Kevin Turbang, https://pygwb.docs.ligo.org/pygwb/

[13] *LISA For Cosmologists: Calculating The Signal-To-Noise Ratio For Stochastic And Deterministic Sources*, Tristan L. Smith, Swarthmore College, tsmith2@swarthmore.edu, R. R. Caldwell, 11-15-2019, https://works.swarthmore.edu/cgi/viewcontent.cgi?article=1378&context=fac-physics

[14] *Stochastic gravitational wave background: methods and Implications*, Nick van Remortel, Kamiel Janssens, Kevin Turbang, 3 Oct 2022, https://arxiv.org/abs/2210.00761

[15] *The NANOGrav 15 yr Data Set: Evidence for a Gravitational-wave Background*, Gabriella Agazie et al, Published June 29 2023, DOI: 10.3847/2041-8213/acdac6 https://iopscience.iop.org/article/10.3847/2041-8213/acdac6

[16] *Galaxies from cosmic dawn to cosmic noon with KLASS,* Charlotte Mason, KMOS@5: Star and Galaxy Formation in 3D — Challenges at KMOS 5th Year, Conference held 3-6 December, 2018 in Garching b. München, Germany. Online at https://www.eso.org/sci/meetings/2018/KMOS2018.html, kmos2018, id.23, Publication Date: December 2018, DOI: 10.5281/zenodo.2595152, https://ui.adsabs.harvard.edu/abs/2018kmos.confE..23M/abstract

[17] *Shouts and Murmurs: Combining Individual Gravitational-wave Sources with the Stochastic Background to Measure the History of Binary Black Hole Mergers*, Tom Callister, Maya Fishbach, Daniel E. Holz, Will M. Farr, June 2020, https://ui.adsabs.harvard.edu/abs/2020ApJ...896L..32C, DOI: 10.3847/2041-8213/ab9743.

[18] *The astrophysical gravitational wave stochastic background*, Tania Regimbau, 2011 National Astronomical Observatories of Chinese Academy of Sciences and IOP Publishing, *Research in Astronomy and Astrophysics*, Volume 11, Number 4, DOI 10.1088/1674-4527/11/4/001, https://iopscience.iop.org/article/10.1088/1674-4527/11/4/001.

[19] GW170817: *Implications for the Stochastic Gravitational-Wave Background from Compact Binary Coalescences*, B. P. Abbott et al, (LIGO Scientific Collaboration and Virgo Collaboration), *Phys. Rev. Lett*, 120, 091101, Published February 28, 2018, https://journals.aps.org/prl/abstract/10.1103/PhysRevLett.120.091101

[20] Thomas Callister, GitHub, https://git.ligo.org/thomas-callister/stochastic-modeling.git (GitHub clone HTTPS), https://git.ligo.org/thomas-callister/stochastic-modeling/-/tree/master/ (main branch link), https://git.ligo.org/thomas-callister/stochastic-modeling/-/tree/master/code (code link and calculation explanation)

[21] Arianna Renzini, GitHub, https://git.ligo.org/pygwb/pygwb.git (GitHub clone HTTPS), https://git.ligo.org/arianna.renzini/pygwb-ssi/-/tree/master/tutorials (main list of tutorials followed), https://git.ligo.org/arianna.renzini/pygwb-ssi/-/tree/master/pygwb (for simulating a CBC background)